Simulation of Convective Energy Transport in the Solar Photosphere

Cand. no. 3

(Dated: May 30, 2023)

We present the results of our HD simulation of convection in the Sun's photosphere. As convection is the primary energy transporter in the outer third of the Sun Stein and Nordlund (2000), we seek to create a model that describes this very behavior. Compared to previous research, e.g. Brun and Miesch (2008), Nordlund *et al.* (2009), our model shows how perturbations in the temperature create convective energy transfer close to the solar surface.

I. Introduction

Observations of the solar granules date back to the days of Galileo Galilei and Christopher Schneier in the early 17th century. With the first photographic recordings of the granulation pattern made by M. Janssen in 1878, the shapes of the granules remained the principal method of investigation for many decades (Kupka and Muthsam 2017). In more present times, the local mixing-length theory was adapted to astrophysical settings (Abbett *et al.* 1996).

As convection is one of the fundamental mechanisms for carrying energy from the stellar interiors to the outermost layers (Pasetto *et al.* 2016), studying our closest star stands out as a golden opportunity to expand the knowledge horizon of humankind. With the numerous numerical simulation models in the late 80s and early 90s (Abbett *et al.* 1996), scientists of today have a vast ocean of research to dive through in the pursuit of more advanced and precise models to describe the life-giving source that is the Sun.

In this paper, we solve the hydrodynamic (HD) equations that describe gas in the solar photosphere numerically. We use the Forward Time Centered Space (FTC) scheme in combination with the upwind scheme to correct for any instabilities. Our main goal is to create a simulation of the fluid that depicts convective energy transfer. As all numerical models are limited by the finite nature of computers, we also explore the errors we expect to see.

We start by describing the computational structure of the model, and the discretization of the HD equations in Section II. Some of the longer derivations are included in Appendix A & B. In Section III, we present and describe our results. This includes snapshots of our simulation for different variables, as well as the time-evolved relative average values. All of our findings are discussed and compared to previous research in Section IV, and we reach our conclusion and experience working on this paper in Section V.

II. Method

A. Algorithm

The equations used in this paper are the continuity equation (CE) (Eq. 1), the momentum equation (ME) (Eq. 2), and the energy equation (EE) (Eq. 3).

$$\frac{\partial \rho}{\partial t} + \nabla \cdot (\rho \mathbf{u}) = 0 \tag{1}$$

$$\frac{\partial \rho \mathbf{u}}{\partial t} + \nabla \cdot (\rho \mathbf{u} \otimes \mathbf{u}) = -\nabla P + \rho \mathbf{g} \tag{2}$$

$$\frac{\partial e}{\partial t} + \nabla \cdot (e \mathbf{u}) = -P \nabla \cdot \mathbf{u} \tag{3}$$

As seen from Eq. 1, the fluid is assumed as incompressible, and thus the mass is conserved. We also assume an ideal gas with the mean molecular mass $\mu = 0.61$ and internal energy

$$e = \frac{\rho k_B T}{(\gamma - 1)\mu m_u} \tag{4}$$

where $\gamma = 5/3$ is the ratio between the specific heats c_P and c_V, $k_B = 1.381 \cdot 10^{-23}\,\mathrm{JK}^{-1}$ is the Boltzmann constant, and $m_u = 1.661 \cdot 10^{-27}$ kg is the atomic mass unit. The unit of internal energy is thus energy per volume. The equation of state (EoS) for an ideal gas is given by

$$P = (\gamma - 1)e \tag{5}$$

We also assume constant gravity inside the computational grid, with $|\mathbf{g}| = GM_\odot / R_\odot^2$. In Appendix A, we derive and explain how we obtain the expressions for the primary variables, which are mass density ρ, horizontal velocity u, vertical velocity w, and internal energy e when the flow $\mathbf{u} = (u, w)$ is assumed to be non-constant. The discretized equations are derived in Appendix B. We use the superscript n to indicate the time, and the subscripts i and j to indicate the position along the x- and y-direction, respectively. For ρ we have

$$\rho_{i,j}^{n+1} = \rho_{i,j}^n + \left[\frac{\partial \rho}{\partial t}\right]_{i,j}^n \Delta t \tag{6}$$

where the time derivative of ρ is given by Eq. B1. The discretized expression for the horizontal velocity u is

$$u_{i,j}^{n+1} = \frac{[\rho u]_{i,j}^n + \left[\frac{\partial \rho u}{\partial t}\right]_{i,j}^n \Delta t}{\rho_{i,j}^{n+1}} \tag{7}$$

where the time derivative of ρu is given by Eq. B3. In the vertical direction, the expression is

$$w_{i,j}^{n+1} = \frac{[\rho w]_{i,j}^n + \left[\frac{\partial \rho w}{\partial t}\right]_{i,j}^n \Delta t}{\rho_{i,j}^{n+1}} \tag{8}$$

where the time derivative term is given by Eq. B8. For the internal energy e, the expression is

$$e_{i,j}^{n+1} = e_{i,j}^n + \left[\frac{\partial e}{\partial t}\right]_{i,j}^n \Delta t \tag{9}$$

with the time derivative given by Eq. B9.

B. Numerical schemes

Though unconditionally unstable (Abbassi 2006), meaning that the numerical errors are certainly produced and grow exponentially (Rezzolla 2020), we use the FTCS scheme when solving the time derivatives of variables that are not affected by the non-constant flow. We then advance the variable forward in time by differencing neighboring points in the computational grid. For a 1D variable ϕ, the FTCS is on the form

$$\left[\frac{\partial \phi}{\partial t}\right]_i^{n+1} \approx \frac{\phi_{i+1}^n - \phi_{i-1}^n}{2\Delta x} \tag{10}$$

However, if a variable is affected by the flow (i.e. by multiplication with either u or w), we use the first-order upwind scheme, which is a stable scheme in the sense that the solutions will not have exponentially growing modes (Rezzolla 2020). This means that the flow determines which point we use when advancing the variable in time. If the flow is positive, we use the previous grid point, and vice versa for negative flow. Applied to the 1D advection equation

$$\left[\frac{\partial \phi}{\partial t}\right]_i^{n+1} = -v_i^n \left[\frac{\partial \phi}{\partial x}\right]_i^n$$

the spatial derivative becomes

$$\left[\frac{\partial \phi}{\partial x}\right]_i^n \approx \begin{cases} \frac{\phi_i^n - \phi_{i-1}^n}{\Delta x} & \text{if} \quad v_i^n \geq 0 \\ \frac{\phi_{i+1}^n - \phi_i^n}{\Delta x} & \text{if} \quad v_i^n < 0 \end{cases} \tag{11}$$

thus taking into account the direction of the flow.

C. Time step length

We determine the optimal step length from the time derivatives of the primary variables. For a primary variable ϕ, we calculate the relative change per time step as

$$\text{rel}(\phi) = \left| \frac{\partial \phi}{\partial t} \cdot \frac{1}{\phi} \right|$$

For the relative change of position, we have

$$\text{rel}(x) = \left| \frac{u}{\Delta x} \right|$$
$$\text{rel}(y) = \left| \frac{w}{\Delta y} \right|$$

For each primary variable and position, we choose the maximum value. Now we have multiple maxima, one for each of the relative changes. From these we choose the maximum again, leaving us with one maximum value δ. The optimal step length Δt is then chosen as

$$\Delta t = \frac{p}{\delta} \tag{12}$$

where p is chosen to be 0.1. This means that the product $\Delta t \cdot \delta$ is equal to p, also known as the Courant-Friedrichs-Lewy condition. One thing to notice is that any zero velocities will destroy this. These zero points are then excluded from the calculations. We also set a lower boundary on the time-step of $\Delta t \geq 0.1$ s, so as to not have unnecessarily small step lengths.

D. The model

1. *Computational grid*

Our model solves the HD equations in a box of length 12 Mm in the horizontal direction, discretized into 300 grid points. The height is 4 Mm in the vertical direction, discretized into 100 grid points. Thus we have a spatial resolution of 0.04 Mm in both directions.

2. *Gaussian perturbation*

In order to provoke the gas to become convectively unstable, we create a 2D Gaussian perturbation, which is added to the initial temperature. We use the 2D Gaussian function

$$f(x,y) = \sum_i^N A_i \exp\left\{ -\left[\frac{(x-x_i)^2}{2\sigma_{xi}^2} + \frac{(y-y_i)^2}{2\sigma_{yi}^2} \right] \right\} \tag{13}$$

where we sum over N surfaces to create a surface with N perturbations.

3. *Initial conditions*

The initial values for temperature and pressure at the top of the computational box are $T^0 = 5778$ K and $P^0 = 1.8 \cdot 10^4$ Pa, respectively. These values are of the Solar photosphere, from Gudiksen (2022). There are two requirements for the initial conditions:

1. The gas needs to be in hydrostatic equilibrium.

2. The double logarithmic gradient

$$\nabla = \frac{\partial \ln T}{\partial \ln P} \tag{14}$$

must be just slightly larger than 2/5.

For an ideal gas, the adiabatic temperature gradient $\nabla_{\rm ad} = 2/5$ (Gudiksen 2022). Convection sets in where and when the temperature gradient becomes larger than $\nabla_{\rm ad}$ (Pasetto *et al.* 2016). In order to ensure convection, we thus set $\nabla = 0.5$. Eq. 14 is solved to find the expression for the change in temperature:

$$\frac{\partial T}{\partial y} = \nabla \frac{T}{P} \frac{\partial P}{\partial y} \tag{15}$$

As gravity is the only force acting on the gas in the box, hydrostatic equilibrium is obtained when

$$\frac{\partial P}{\partial y} = -|\mathbf{g}|\rho \tag{16}$$

We then integrate the equations numerically with the forward Euler (FE) scheme to obtain[1]

$$T^0_{i,j+1} = T^0_{i,j} - \frac{\partial T}{\partial y}\Delta y \tag{17}$$

$$P^0_{i,j+1} = P^0_{i,j} - \frac{\partial P}{\partial y}\Delta y \tag{18}$$

From these equations, the initial values for e and ρ are calculated with Eqs. 5 & 4, respectively, and in that order.

4. Boundary conditions

After the optimal time step has been calculated, the primary variables ρ, u, w, and e are advanced in time. Since the discretized HD equations cannot be solved at the endpoints of the grid, i.e. at $i = 0$ and $j = 0$, and at $i = N_x - 1$ and $j = N_y - 1$, we apply boundary conditions at said points. Derivatives on the boundaries are set by the 3-point difference approximation

$$\left[\frac{\partial \phi}{\partial y}\right]^n_{i,j} \approx \pm \frac{3\phi^n_{i,j} - 4\phi^n_{i,j\pm1} + \phi^n_{i,j\pm2}}{2\Delta y} \tag{19}$$

where we use $(-)$ at $j = N_y - 1$, and $(+)$ at $j = 0$.

- **Horizontal boundary**
  Each primary variable ϕ has periodic boundary conditions in the horizontal direction, i.e.

$$\phi^n_{-1,j} = \phi^n_{N_x-1,j}$$
$$\phi^n_{N_x,j} = \phi^n_{0,j}$$

[1] Here, the temperature is assumed to be the temperature after we add the Gaussian perturbation.

- **Vertical boundary: Horizontal velocity**
  The vertical gradient of the horizontal component of the velocity is zero at the boundary. This means that Eq. 19 is equal to zero, and that

$$u^n_{i,0} = \frac{4u^n_{i,1} - u^n_{i,2}}{3}$$
$$u^n_{i,N_y-1} = \frac{4u^n_{i,N_y-2} - u^n_{i,N_y-3}}{3}$$

- **Vertical boundary: Vertical velocity**
  The vertical component of the vertical velocity is zero at the boundaries:

$$w^n_{i,0} = w^n_{i,N_y-1} = 0$$

- **Vertical boundary: Mass density and energy**
  Hydrostatic equilibrium must be fulfilled at the boundaries, i.e. Eq. 16 is valid. From the EoS, we get

$$\frac{\partial e}{\partial y} = (\gamma - 1)^{-1} \frac{\partial P}{\partial y}$$

Solving this with the 3-point approximation, we find the expression for the boundary condition for e, which in turn is used to determine the boundary condition for ρ from the ideal gas equation (Eq. 4).

III. Results

Figure 1 shows the 2D Gaussian perturbation we add to the initial temperature. The parameters used to create this surface are listed in Table I. In Figure 2, we present snapshots from our simulation of convective transport, at 1 s, 3 min, 6 min, and 9 min. The left panel shows the temperatures in K, whilst the right panel shows the corresponding speeds in ms^{-1}. In the upper left figure, a snapshot at $t = 1$ s is shown. We see that the gas flows toward the centers of the perturbations, with a higher velocity towards perturbations closer to the surface. Below the peaks of the Gaussian perturbations, the gas has higher speeds. This is also seen in the corresponding speed figure to the upper right. The second row from the top of Figure 2 shows the snapshot

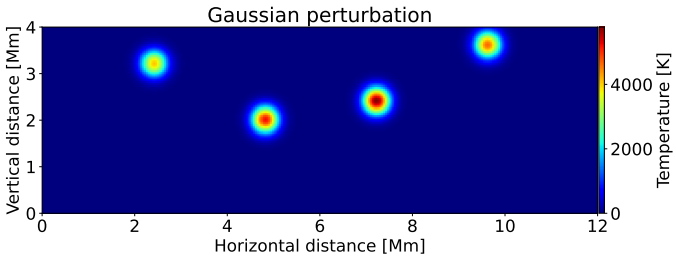

Figure 1: A 2D Gaussian perturbation with four peaks. This is added to the initial temperature in order to obtain convective instability.

(a) 2D temperature plots on top of velocity.

(b) 2D speed plots on top of velocity.

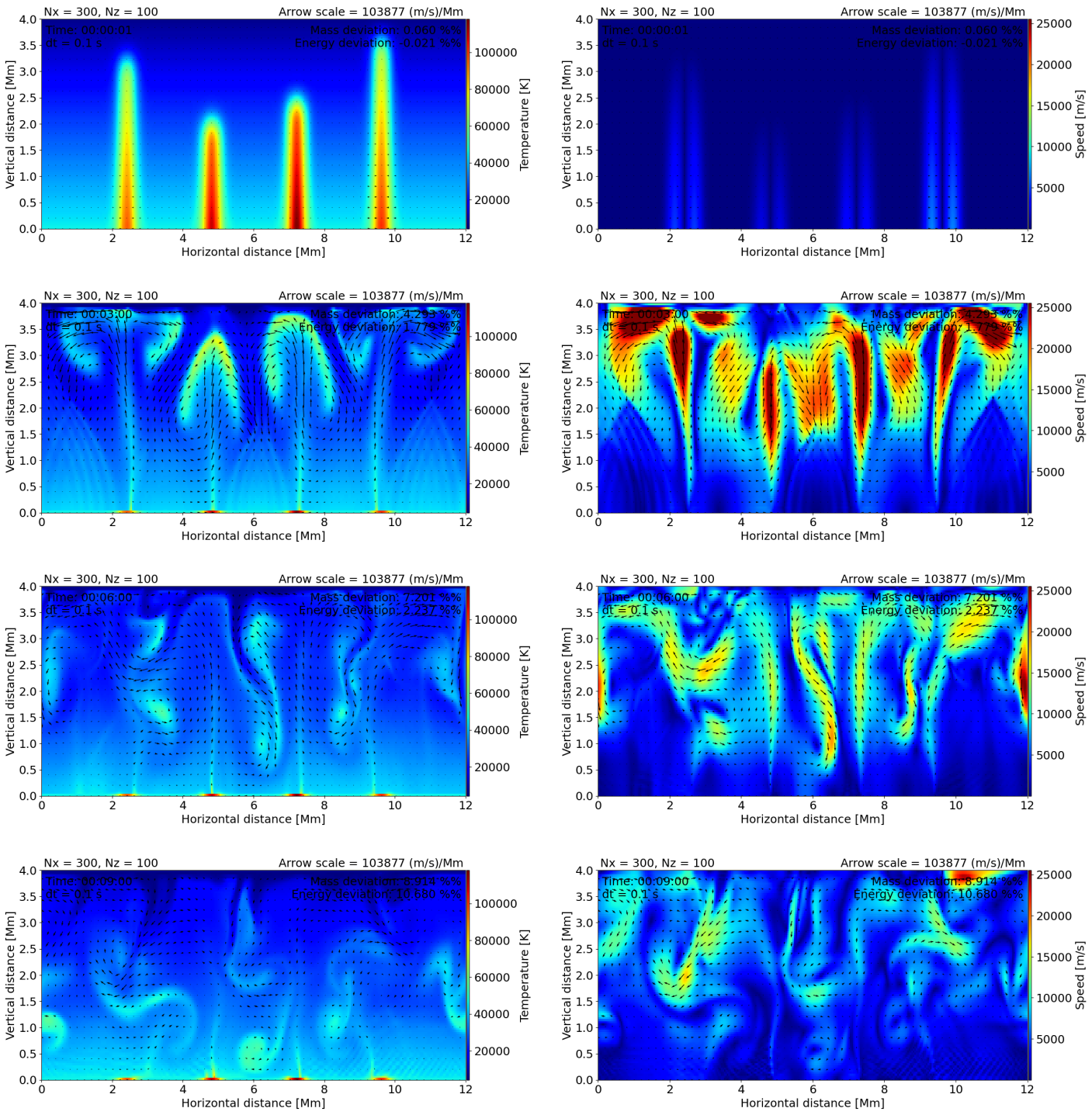

Figure 2: Snapshots of a convective transport simulation at times 1 s, 4 min, 6 min, and 9 min from the top. **a)** Temperatures in K in the computational box in colors and velocity vectors. **b)** Speeds ($\sqrt{u^2 + w^2}$) in ms^{-1} and the velocity vectors.

at $t = 3$ min, and we see that hot gas (light colors) moves towards the surface and cool gas (dark colors) flows downwards, indicating convective transport of energy (Brun and Miesch 2008). One can see that the speed is highest when the gas moves in the vertical direction from the corresponding speed figure. The figures in the third row from the top show the snapshots at $t = 6$ min. Downdrafts are formed and visible as the dark blue regions extending downwards from the surface. The last snapshots at $t = 9$ min are shown in the lower row of Figure 2, and depict the gas velocity set-

Parameters for the 2D Gaussian perturbation

A [K]	$(\mathbf{x_0}, \mathbf{y_0})$ [Mm]	$(\sigma_\mathbf{x}, \sigma_\mathbf{y})$ [Mm]
4044.6	(2.4, 3.2)	(0.2, 0.2)
5200.2	(4.8, 2.0)	(0.2, 0.2)
5778.0	(7.2, 2.4)	(0.2, 0.2)
4622.4	(9.6, 3.6)	(0.2, 0.2)

Table I: Amplitudes, peak center, and standard deviations for the 2D Gaussian perturbation shown in Figure 1.

tling. Downdrafts are still visible as darker regions close to the surface, and higher temporal gas is now located deeper down in the simulation box. As seen from the lower left figure, the cooled gas moving in the downwards direction has higher velocities than the hotter upwards-flowing gas.

In Figure 3, the average values for temperature and speed through the simulation are shown. The temperature rel-

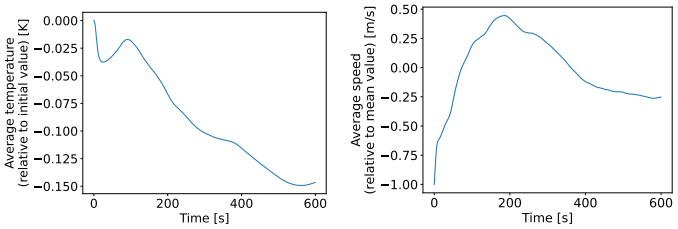

Figure 3: Time evolution of the average values for temperature relative to the initial value (left) in K, and speed relative to the mean value (right) in ms^{-1}.

ative to the initial temperature shows a decreasing trend, with a slight increase around 160 s. At the end of the simulation, the temperature has decreased by 15%, relative to the initial temperature. As the speed is zero at the beginning of the computation, the average values are shown relative to the mean value instead of the initial value. We see that the average grows towards nearly 50% increase at around 200s, before flattening out towards the end of the simulation.

One thing to note is that both the mass and internal energy deviate through the simulation. The mass and internal energy have deviated with 0.06% and -0.021%, respectively after 1 second. After 4 min, the deviations have grown to 5.047% for the mass, and 6.24% for the energy. The final snapshot of the simulation shows that the mass has deviated by 8.72%, and the energy by 6.467%. These deviations are percentages of the initial values. In Figure 4, the time evolved average of the mass density relative to the initial value is shown in the left panel, in kgm^{-1}. The curve shows a linear growth trend from the beginning of the simulation, before flattening out to a value of around 9% towards the end. The time-evolved average values for the internal energy in Jm^{-3} are shown in the right panel of Figure 4. The curve dips from the beginning, before increasing from approximately 100 s. From here, the curve has two maxima at around 250 s and 550 s with relative averages of $\sim 7\%$ and $\sim 1.1\%$, respectively. Between them is a minimum point of approximately 1% at $t = 400$ s.

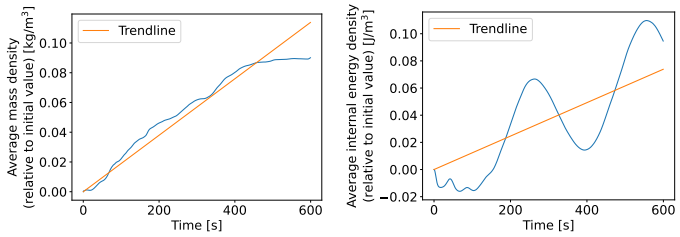

Figure 4: Time evolution of the average values for mass density (left) in kgm^{-3} and internal energy (right) in Jm^{-3} relative to their initial values. Included are also the trendlines.

IV. Discussion

With the Gaussian perturbations sown in Figure 1, we see that the time evolution of the temperatures and speeds in Figure 2 are in agreement with Stein and Nordlund (2000), which describe the convective flow as *"somewhat like a fountain"*. The inward flow described at the beginning of the simulation can be explained by the underpressure created by the ascending gas. Our snapshots show the same gas motion as described in Meakin and Arnett (2007). They simulate the convective layer of the Sun, but it is our understanding that the convective motions should be similar to our simulation of convective motion in the solar photosphere. As stated by Nordlund *et al.* (2009), the ascending gas is cooled at the top, and descending gas is re-heated at the bottom. This behavior is clearly visible in Figure 2. In their simulations, Stein and Nordlund (1998) finds that the temperature close to the solar surface ranges from 5000 K to 10^4 K. Our simulation correlates with this when the convective transport is greatest.

When it comes to the numerical solutions we present, numerous papers have been written on the topic, e.g. Chouliaras and Gourgouliatos (2022), Kupka and Muthsam (2017), Pasetto *et al.* (2016). Especially relevant to this paper is the choice and implementation of the numerical scheme. As previously mentioned, the FTCS is unconditionally stable, while the upwind scheme is stable (Abbassi 2006). Chouliaras and Gourgouliatos (2022) shows that with the use of the upwind scheme, an improvement of two orders of magnitude can be obtained for their case of study. This is compared to the FTCS. In our results, we see that the mass density and energy deviate from the initial values. As the numerical schemes are approximations, some errors are expected. In the average mass density plot of Figure 4, the trend is linear. As the CE is expected to conserve the mass, this deviation arises from computational limitations. In Rezzolla (2020), the errors of the FTCS and upwind schemes are stated to be of orders $\mathcal{O}(\Delta t, \Delta x^2)$ and $\mathcal{O}(\Delta t, \Delta x)$, respectively. The linearity trend of the mass density deviation is in agreement with this. For the internal energy, the deviation has a more oscillating curve,

however, but the trend is also linear. Another aspect is the fact that our time step dt is always the lower threshold of 0.1 s. This can also contribute to errors that might hide between our numerical resolution.

V. Conclusion

In this paper, we have solved the HD equations for the solar photosphere, and simulated convective energy transport in two dimensions. With the 2D Gaussian perturbation added to the initial temperature, we saw clear signs of convection (Brun and Miesch 2008). Given the finite precision of computers, we also briefly analyzed our results and compared them to the numerical scheme analysis done on the FTCS and upwind schemes by Rezzolla (2020), and the stability analysis performed by Abbassi (2006). In conclusion, we found that our simulation was in agreement with previous research done by e.g. Nordlund *et al.* (2009), Kupka and Muthsam (2017).

Further research may include the solar magnetic field, i.e. magnetohydrodynamics. Also, experimenting with more precise numerical schemes could improve the results. Since we noticed that our time step remained at our lower threshold, performing heavier computations with smaller dt is recommended.

During the production of this paper, we met some challenges in the implementation and understanding of the numerical schemes. The author especially had a hard time mentally visualizing how the resulting simulation should look. One clear indicator that something had to be wrong was of course that the simulation crashed after < 1 min. With excellent help from T.A. and fellow students, the final computational implementation could run for 20 min (probably longer, but since there was little interest after 10 min, we did not proceed with even longer simulations[2]) without crashing.

[2] I know what you're thinking: *"Where is the scientific curiosity?"* Rest assured that I have every intention of doing so at a less deadline-dominated time.

APPENDICES

A. Decomposing the equations

We split the Eqs. 1-3 into x and y components. Note that $\mathbf{u} = (u, w)$, i.e. u in the x direction and w in the y direction. First of all, the ∇-operator is written as

$$\nabla = \left(\frac{\partial}{\partial x}, \frac{\partial}{\partial y}\right)$$

Starting with the CE, we get

$$\begin{aligned} \frac{\partial \rho}{\partial t} + \nabla \cdot (\rho \mathbf{u}) &= 0 \\ \frac{\partial \rho}{\partial t} + \frac{\partial \rho u}{\partial x} + \frac{\partial \rho w}{\partial y} &= 0 \\ \Rightarrow \frac{\partial \rho}{\partial t} &= -\frac{\partial \rho u}{\partial x} - \frac{\partial \rho w}{\partial y} \end{aligned}$$

For the ME, we have

$$\frac{\partial \rho \mathbf{u}}{\partial t} + \nabla \cdot (\rho \mathbf{u} \otimes \mathbf{u}) = -\nabla P + \rho \mathbf{g} \tag{A1}$$

The outer product gives

$$\rho \mathbf{u} \otimes \mathbf{u} = \begin{bmatrix} \rho u^2 & \rho u w \\ \rho u w & \rho w^2 \end{bmatrix},$$

where $\mathbf{u} = (u, w)$, i.e. u in the x direction and w in the y direction. Now, we split Eq. A1 into x and y. For x, we get

$$\begin{aligned} \frac{\partial \rho u}{\partial t} + \frac{\partial \rho u^2}{\partial x} + \frac{\partial \rho u w}{\partial y} &= -\frac{\partial P}{\partial x} \\ \Rightarrow \frac{\partial \rho u}{\partial t} &= -\frac{\partial \rho u^2}{\partial x} - \frac{\partial \rho u w}{\partial y} - \frac{\partial P}{\partial x} \end{aligned}$$

In the y direction, we get

$$\begin{aligned} \frac{\partial \rho w}{\partial t} + \frac{\partial \rho w^2}{\partial y} + \frac{\partial \rho u w}{\partial x} &= -\frac{\partial P}{\partial y} + \rho g_y \\ \Rightarrow \frac{\partial \rho w}{\partial t} &= -\frac{\partial \rho w^2}{\partial y} - \frac{\partial \rho u w}{\partial x} - \frac{\partial P}{\partial y} + \rho g_y \end{aligned}$$

The gravitational force only affects the y-direction, as this is the same direction as the radial direction. Finally, the EE becomes

$$\begin{aligned} \frac{\partial e}{\partial t} + \nabla \cdot (e \mathbf{u}) &= -P \nabla \cdot \mathbf{u} \\ \frac{\partial e}{\partial t} + \frac{\partial e u}{\partial x} + \frac{\partial e w}{\partial y} &= -P\left(\frac{\partial u}{\partial x} + \frac{\partial w}{\partial y}\right) \\ \Rightarrow \frac{\partial e}{\partial t} &= -\frac{\partial e u}{\partial x} - \frac{\partial e w}{\partial y} - P\left(\frac{\partial u}{\partial x} + \frac{\partial w}{\partial y}\right) \end{aligned}$$

B. Calculating the approximations of the time derivatives of the primary variables

1. Continuity equation

For the CE, we have

$$\left[\frac{\partial \rho}{\partial t}\right]^n_{i,j} = -\rho^n_{i,j}\left(\left[\frac{\partial u}{\partial x}\right]^n_{i,j} + \left[\frac{\partial w}{\partial y}\right]^n_{i,j}\right) - u^n_{i,j}\left[\frac{\partial \rho}{\partial x}\right]^n_{i,j} - w^n_{i,j}\left[\frac{\partial \rho}{\partial y}\right]^n_{i,j} \tag{B1}$$

where n is the time index and (i,j) are the positional indices. Here,

$$\left[\frac{\partial u}{\partial x}\right]^n_{i,j} \approx \frac{u^n_{i+1,j} - u^n_{i-1,j}}{2\Delta x}$$
$$\left[\frac{\partial w}{\partial y}\right]^n_{i,j} \approx \frac{w^n_{i+1,j} - w^n_{i-1,j}}{2\Delta y}$$
$$\left[\frac{\partial \rho}{\partial x}\right]^n_{i,j} \approx \begin{cases} \frac{\rho^n_{i,j} - \rho^n_{i-1,j}}{\Delta x} & \text{if} \quad u^n_{i,j} \geq 0 \\ \frac{\rho^n_{i+1,j} - \rho^n_{i,j}}{\Delta x} & \text{if} \quad u^n_{i,j} < 0 \end{cases}$$
$$\left[\frac{\partial \rho}{\partial y}\right]^n_{i,j} \approx \begin{cases} \frac{\rho^n_{i,j} - \rho^n_{i,j-1}}{\Delta y} & \text{if} \quad w^n_{i,j} \geq 0 \\ \frac{\rho^n_{i,j+1} - \rho^n_{i,j}}{\Delta y} & \text{if} \quad w^n_{i,j} < 0 \end{cases}$$

Then, the primary variable ρ is advanced in time by

$$\rho^{n+1}_{i,j} = \rho^n_{i,j} + \left[\frac{\partial \rho}{\partial t}\right]^n_{i,j} \Delta t \tag{B2}$$

where Eq. B1 is inserted into $\left[\frac{\partial \rho}{\partial t}\right]^n_{i,j}$.

2. Momentum equation

a. *Horizontal equation*

The ME is split up into a horizontal and vertical equation. The horizontal equation is

$$\begin{aligned}\left[\frac{\partial \rho u}{\partial t}\right]^n_{i,j} = &- [\rho u]^n_{i,j} \left(\left[\frac{\partial u}{\partial x}\right]^n_{i,j} + \left[\frac{\partial w}{\partial y}\right]^n_{i,j} \right) - u^n_{i,j} \left[\frac{\partial \rho u}{\partial x}\right]^n_{i,j} \\ &- w^n_{i,j} \left[\frac{\partial \rho u}{\partial y}\right]^n_{i,j} - \left[\frac{\partial P}{\partial x}\right]^n_{i,j}\end{aligned} \tag{B3}$$

where

$$\left[\frac{\partial u}{\partial x}\right]^n_{i,j} \approx \begin{cases} \frac{u^n_{i,j} - u^n_{i-1,j}}{\Delta x} & \text{if} \quad u^n_{i,j} \geq 0 \\ \frac{u^n_{i+1,j} - u^n_{i,j}}{\Delta x} & \text{if} \quad u^n_{i,j} < 0 \end{cases}$$
$$\left[\frac{\partial w}{\partial y}\right]^n_{i,j} \approx \frac{w^n_{i,j+1} - w^n_{i,j-1}}{2\Delta y}$$
$$\left[\frac{\partial \rho u}{\partial x}\right]^n_{i,j} \approx \begin{cases} \frac{[\rho u]^n_{i,j} - [\rho u]^n_{i-1,j}}{\Delta x} & \text{if} \quad u^n_{i,j} \geq 0 \\ \frac{[\rho u]^n_{i+1,j} - [\rho u]^n_{i,j}}{\Delta x} & \text{if} \quad u^n_{i,j} < 0 \end{cases}$$
$$\left[\frac{\partial \rho u}{\partial y}\right]^n_{i,j} \approx \begin{cases} \frac{[\rho u]^n_{i,j} - [\rho u]^n_{i,j-1}}{\Delta y} & \text{if} \quad w^n_{i,j} \geq 0 \\ \frac{[\rho u]^n_{i,j+1} - [\rho u]^n_{i,j}}{\Delta y} & \text{if} \quad w^n_{i,j} < 0 \end{cases}$$
$$\left[\frac{\partial P}{\partial x}\right]^n_{i,j} \approx \frac{P^n_{i+1,j} - P^n_{i-1,j}}{2\Delta x}$$

The time-evolved equation thus becomes

$$\left[\frac{\partial \rho u}{\partial t}\right]^n_{i,j} \approx \frac{[\rho u]^{n+1}_{i,j} - [\rho u]^n_{i,j}}{\Delta t}$$

which can be re-written to

$$u^{n+1}_{i,j} = \frac{[\rho u]^n_{i,j} + \left[\frac{\partial \rho u}{\partial t}\right]^n_{i,j} \Delta t}{\rho^{n+1}_{i,j}} \tag{B4}$$

since we already know $\rho^{n+1}_{i,j}$. The expression for the time derivative of $[\rho u]^n_{i,j}$ is given by Eq. B3.

b. Vertical equation

The vertical equation for the ME is

$$\frac{\partial \rho w}{\partial t} = -\frac{\partial \rho w^2}{\partial y} - \frac{\partial \rho u w}{\partial x} - \frac{\partial P}{\partial y} + \rho g_y \tag{B5}$$

as derived in Appendix A. Using the chain rule on the two first terms on the right-hand side, we get

$$\begin{aligned}\frac{\partial \rho w}{\partial t} &= -\rho w \frac{\partial w}{\partial y} - w\frac{\partial \rho w}{\partial y} - \rho w \frac{\partial u}{\partial x} - u\frac{\partial \rho w}{\partial x} - \frac{\partial P}{\partial y} + \rho g_y \\ &= -\rho w \left(\frac{\partial u}{\partial x} + \frac{\partial w}{\partial y}\right) - u\frac{\partial \rho w}{\partial x} - w\frac{\partial \rho w}{\partial y} - \frac{\partial P}{\partial y} + \rho g_y\end{aligned} \tag{B6}$$

Now we can express Eq. B6 as

$$\begin{aligned}\left[\frac{\partial \rho w}{\partial t}\right]^n_{i,j} = &- [\rho w]^n_{i,j}\left(\left[\frac{\partial u}{\partial x}\right]^n_{i,j} + \left[\frac{\partial w}{\partial y}\right]^n_{i,j}\right) - u^n_{i,j}\left[\frac{\partial \rho w}{\partial x}\right]^n_{i,j} \\ &- w^n_{i,j}\left[\frac{\partial \rho w}{\partial y}\right]^n_{i,j} - \left[\frac{\partial P}{\partial y}\right]^n_{i,j} + \rho^n_{i,j}\, g_y\end{aligned} \tag{B7}$$

As we now operate in the vertical direction, the term $\left[\frac{\partial u}{\partial x}\right]^n_{i,j}$, which is strictly in the x-direction, will be treated with central space. Also, the pressure term does not have a velocity factor working on it, so central space is used on that as well. The rest of the terms are all multiplied with velocities, so here we use the upwind scheme. We thus get

$$\begin{aligned}\left[\frac{\partial u}{\partial x}\right]^n_{i,j} &\approx \frac{u^n_{i+1,j} - u^n_{i-1,j}}{2\Delta x} \\ \left[\frac{\partial w}{\partial y}\right]^n_{i,j} &\approx \begin{cases} \frac{w^n_{i,j} - w^n_{i,j-1}}{\Delta y} & \text{if} \quad w^n_{i,j} \geq 0 \\ \frac{w^n_{i,j+1} - w^n_{i,j}}{\Delta y} & \text{if} \quad w^n_{i,j} < 0 \end{cases} \\ \left[\frac{\partial \rho w}{\partial x}\right]^n_{i,j} &\approx \begin{cases} \frac{[\rho w]^n_{i,j} - [\rho w]^n_{i-1,j}}{\Delta x} & \text{if} \quad u^n_{i,j} \geq 0 \\ \frac{[\rho w]^n_{i+1,j} - [\rho w]^n_{i,j}}{\Delta x} & \text{if} \quad u^n_{i,j} < 0 \end{cases} \\ \left[\frac{\partial \rho w}{\partial y}\right]^n_{i,j} &\approx \begin{cases} \frac{[\rho w]^n_{i,j} - [\rho w]^n_{i,j-1}}{\Delta y} & \text{if} \quad w^n_{i,j} \geq 0 \\ \frac{[\rho w]^n_{i,j+1} - [\rho w]^n_{i,j}}{\Delta y} & \text{if} \quad w^n_{i,j} < 0 \end{cases} \\ \left[\frac{\partial P}{\partial y}\right]^n_{i,j} &\approx \frac{P^n_{i,j+1} - P^n_{i,j-1}}{2\Delta y}\end{aligned}$$

Following the same logic as in Appendix B 2 a, we get

$$w^{n+1}_{i,j} = \frac{[\rho w]^n_{i,j} + \left[\frac{\partial \rho w}{\partial t}\right]^n_{i,j} \Delta t}{\rho^{n+1}_{i,j}} \tag{B8}$$

where $\left[\frac{\partial \rho w}{\partial t}\right]^n_{i,j}$ is given by Eq. B8.

3. Energy equation

As derived in Appendix A, the EE is

$$\frac{\partial e}{\partial t} = -\frac{\partial e u}{\partial x} - \frac{\partial e w}{\partial y} - P\left(\frac{\partial u}{\partial x} + \frac{\partial w}{\partial y}\right)$$

With the chain rule again, we find

$$\begin{aligned}\frac{\partial e}{\partial t} &= -e\frac{\partial u}{\partial x} - u\frac{\partial e}{\partial x} - e\frac{\partial w}{\partial y} - w\frac{\partial e}{\partial y} - P\left(\frac{\partial u}{\partial x} + \frac{\partial w}{\partial y}\right) \\ &= -(e+P)\left(\frac{\partial u}{\partial x} + \frac{\partial w}{\partial y}\right) - u\frac{\partial e}{\partial x} - w\frac{\partial e}{\partial y}\end{aligned}$$

which we write as

$$\left[\frac{\partial e}{\partial t}\right]^n_{i,j} = -\left(e^n_{i,j} + P^n_{i,j}\right)\left(\left[\frac{\partial u}{\partial x}\right]^n_{i,j} + \left[\frac{\partial w}{\partial y}\right]^n_{i,j}\right) - u^n_{i,j}\left[\frac{\partial e}{\partial x}\right]^n_{i,j} - w^n_{i,j}\left[\frac{\partial e}{\partial y}\right] \tag{B9}$$

Here, only the differentials of the internal energy are calculated with the upwind scheme, as they are multiplied by the velocities. We get

$$\begin{aligned}
\left[\frac{\partial u}{\partial x}\right]^n_{i,j} &\approx \frac{u^n_{i+1,j} - u^n_{i-1,j}}{2\Delta x} \\
\left[\frac{\partial w}{\partial y}\right]^n_{i,j} &\approx \frac{w^n_{i,j+1} - w^n_{i,j-1}}{2\Delta y} \\
\left[\frac{\partial e}{\partial x}\right]^n_{i,j} &\approx \begin{cases} \frac{e^n_{i,j} - e^n_{i-1,j}}{\Delta x} & \text{if} \quad u^n_{i,j} \geq 0 \\ \frac{e^n_{i+1,j} - e^n_{i,j}}{\Delta x} & \text{if} \quad u^n_{i,j} < 0 \end{cases} \\
\left[\frac{\partial e}{\partial y}\right]^n_{i,j} &\approx \begin{cases} \frac{e^n_{i,j} - e^n_{i,j-1}}{\Delta y} & \text{if} \quad w^n_{i,j} \geq 0 \\ \frac{e^n_{i,j+1} - e^n_{i,j}}{\Delta y} & \text{if} \quad w^n_{i,j} < 0 \end{cases}
\end{aligned}$$

The time-advanced equation then becomes

$$e^{n+1}_{i,j} = e^n_{i,j} + \left[\frac{\partial e}{\partial t}\right]^n_{i,j} \Delta t \tag{B10}$$

where the time derivative of the energy is given by Eq. B9.

References

Abbassi, N. M. (2006), "Solving the advective PDE in explicit FTC, Lax, Implicit FTC and Crank-Nicholson methods for constant and varying speed." https://www.12000.org/my_notes/advection_PDE/final_solution.htm#x1-190003.1, Accessed: 2023-05-26.

Abbett, W. P., M. Beaver, B. Davids, *et al.* (1996), ApJ **480**, 395.

Brun, A. S., and M. S. Miesch (2008), "STELLAR CONVECTION: Theory and Models," http://lcd-www.colorado.edu/sabrun/StellarConvection_26April08.pdf, Accessed: 2023-05-27.

Chouliaras, G., and K. N. Gourgouliatos (2022), Astron. Comput. **39**.

Gudiksen, B. V. (2022), "AST3310: Astrophysical plasma and stellar interiors," Lecture notes.

Kupka, F., and H. J. Muthsam (2017), Living Rev. Comput. Astrophys. **3** (1).

Meakin, C. A., and D. Arnett (2007), ApJ **667**, 448.

Nordlund, , R. F. Stein, and M. Asplund (2009), Living Rev. Sol. Phys. **6** (2).

Pasetto, S., C. Chiosi, E. Chiosi, M. Cropper, and A. Weiss (2016), MNRAS **459** (3), 3182.

Rezzolla, L. (2020), "Numerical methods for the solution of partial differential equations," /https://itp.uni-frankfurt.de/~rezzolla/lecture_notes/2010/fd_evolution_pdes_lnotes.pdf, Accesed: 2023-05-26.

Stein, R., and Nordlund (1998), ApJ **499**, 914.

Stein, R. F., and Nordlund (2000), Sol. Phys. **192**, 91.